

MANEUVER PERFORMANCE ASSESSMENT OF THE CASSINI SPACECRAFT THROUGH EXECUTION-ERROR MODELING AND ANALYSIS

Sean Wagner*

The Cassini spacecraft has executed nearly 300 maneuvers since 1997, providing ample data for execution-error model updates. With maneuvers through 2017, opportunities remain to improve on the models and remove biases identified in maneuver executions. This manuscript focuses on how execution-error models can be used to judge maneuver performance, while providing a means for detecting performance degradation. Additionally, this paper describes Cassini's execution-error model updates in August 2012. An assessment of Cassini's maneuver performance through OTM-368 on January 5, 2014 is also presented.

INTRODUCTION

The Cassini spacecraft was launched in October 1997 and entered a Saturn orbit in July 2004. After touring Saturn and its moons for nearly a decade, Cassini continues to operate within expectations, particularly with the performance of propulsive burns. Cassini has performed nearly 300 maneuvers since launch through the first half of the Solstice Mission, the final extension of Cassini's tour of Saturn, providing ample data for execution-error modeling and analysis. Cassini accomplishes maneuvers through the use of two independent propulsion systems for trajectory corrections called Orbit Trim Maneuvers (OTMs); the bi-propellant Main Engine Assembly (MEA) for performing large burns and the Reaction Control System (RCS) thrusters for small burns. With the Cassini Solstice Mission concluding in September 2017, safeguarding the performance of Cassini's propulsion and attitude control systems has become a high priority. Reconstructions of the executed maneuvers by the Cassini Navigation Team are utilized to assess the performance of the main engine and RCS thrusters. From such assessments, it is possible to develop reasonable models of the maneuver execution errors, particularly in ΔV magnitude and pointing, and to identify biases seen in the maneuver executions. Execution-error biases, in some cases, can be removed through calibrations of certain flight software parameters or through the maneuver designs themselves. Representative models of the maneuver execution errors can be used to understand future maneuver performance, while providing means for detecting degradation in either propulsion or attitude control. The methodologies that are discussed are not limited to Cassini; they can also be used to evaluate and characterize the maneuver performance of other spacecraft.

Reference 1 documented the Gates execution-error models² employed by Cassini from launch through the four-year Prime Mission, along with the development of the execution-error model used in operations beginning in 2008, from an analysis of nearly ten years of maneuver data (1998–2007). This previous paper also described the processing and analysis of the maneuver data via software developed by the Cassini Maneuver Team. This manuscript focuses on the applications of execution-error analysis and modeling, particularly in judging future maneuver performance and in detecting performance degradation, the latter application becoming more important as Cassini reaches the end of its lifetime. Also, this paper documents the execution-error model updates for main engine and RCS maneuvers from 2009 to 2012.

*Author is a member of the Flight Path Control Group and the Cassini Navigation Team, Jet Propulsion Laboratory, California Institute of Technology; *Mailing Address*: Jet Propulsion Laboratory, Mail Stop 230-205, 4800 Oak Grove Drive, Pasadena, CA 91109-8099; *Tel*: (818) 393-5972; *Fax*: (818) 393-4215; *E-mail address*: Sean.V.Wagner@jpl.nasa.gov

In August 2012, the main engine execution-error model was updated based on the performance of main engine maneuvers following Cassini propulsion's fuel-side repressurization in January 2009.³ A fixed-magnitude bias was identified in the execution of main engine burns, reflecting the observed deficiency in the length of main engine maneuvers. This bias was removed from the execution of main engine maneuvers through a flight parameter change to increase the time of the burns. This change is described in a later section.

In March 2009, Cassini's RCS thrusters were swapped from the main A-branch (set of eight thrusters) to the redundant B-branch thrusters (identical set of eight thrusters) due to the marked degradation in performance of two thrusters on A-branch.^{4,5} In September 2012, a new RCS execution-error model was used in operations, the first model to characterize the execution errors seen with RCS burns on the B-branch thrusters.⁶ Fixed and proportional biases in RCS burn magnitudes were identified on the B-branch thrusters, and both magnitude biases are now removed within the maneuver design process. By comparing the executions of current maneuvers to an existing maneuver execution-error model, early indications of degraded performance in propulsion or attitude control can be observed. In the case of RCS burns, Navigation would have likely seen signs of the thruster degradation on the A-branch. This RCS thruster degradation example is presented, along with various methods for assessing maneuver performance through execution-error modeling and analysis.

A preliminary assessment of these execution-error model updates, designated 2012-1, was made using maneuver data from August 2012 through July 2013 and is documented in Reference 7. Incorporating additional maneuver data through January 5, 2014, this paper will also present an updated assessment of the execution-error models. Based on this new maneuver performance study, it is recommended that the 2012-1 execution-error models remain in use and to maintain the associated maneuver execution adjustments.

MOTIVATIONS FOR EXECUTION-ERROR ANALYSIS

There are several advantages to improving on pre-launch and early in-flight execution-error models. The greatest benefit is probably through improved predictions of fuel usage in future tour segments. In operations, an updated model provides a better *a priori* estimate for OD estimates of maneuvers. Once an OD estimate is available for an executed maneuver, the updated model also provides a better means to assess the maneuver performance. For example, if a maneuver estimate is more than $2\text{-}\sigma$ from the expected ΔV magnitude, a closer examination of the performance of the maneuver is warranted. This maneuver performance assessment is more meaningful if the model is based on a sufficient set of performed maneuvers. A pre-launch or early in-flight model is useful for a rough ΔV usage study of future maneuvers in tour planning, but these models would be poor choices for evaluating performance during maneuver operations.

A gross under-performance of a maneuver may be an early indication of a degraded engine or thruster. Methods for detecting degradation by comparing an under-performed maneuver to an accepted execution-error model are discussed in later sections. Also, the updated model provides more accurate predictions of the post-maneuver trajectory dispersions so that, for example, project scientists may better assess how their observations will be affected.

By continually folding in new maneuver data, computed execution-error biases in magnitude and pointing from the execution-error modeling process may become apparent or previously observed biases may change notably. Significant modifications to a spacecraft's performance may change the model and introduce new execution-error biases (e.g., the switch from A-branch to B-branch thrusters for Cassini's RCS burns). These identified biases can then be compensated for in the maneuver design process or effectively removed via flight software parameter changes or patches (e.g., Cassini's main engine proportional-magnitude bias can be removed by adjusting the main engine accelerometer scale factor). Removing biases can potentially decrease future maneuver execution errors, leading to more maneuver cancellations.

CURRENT MODELS FOR EXECUTION ERRORS

The Gates model has been used to develop the execution-error models for Cassini’s main engine and RCS maneuvers. The Gates execution-error model accounts for four independent error sources: fixed and proportional-magnitude errors and fixed and proportional-pointing errors.² The direction of pointing errors is assumed to have a uniform distribution across 360°. Each of the four sources is assumed to have a Gaussian distribution, so each parameter represents the standard deviation for that error source and each error source is assumed to have a zero mean, once computed biases have been removed from the estimates. Via a weighted maximum-likelihood estimator (see Appendix B), the Gates execution-error model parameters and corresponding biases in execution for the main engine and RCS maneuvers, processed separately, are computed. These two components are tied together; the execution-error model assumes that all (or some) of the biases have been removed. For Cassini pointing errors, a pointing per-axis model is used. An alternative, but equivalent, pointing model was used for the GRAIL, referred to as the total pointing model in Reference 8.

Updates to the execution-error models for Cassini’s main engine and RCS maneuvers were developed and first used in maneuver operations in August 2012,^{3,6} replacing the previous 2008-01 model.⁹ In conjunction with these execution-error model updates, magnitude biases were removed either through a flight parameter change or within the maneuver design process. Identified pointing biases were not extracted, but are accounted for in the execution-error models.

Table 1: 2012-1 Execution-Error Models ($1-\sigma$)

		Main Engine (≤ 13 m/s)	RCS (≤ 0.3 m/s)
Magnitude	Proportional (%)	0.02	0.4
	Fixed (mm/s)	3.5	0.5
Pointing (per axis)	Proportional (mrad)	1.0	4.5
	Fixed (mm/s)	5.0	0

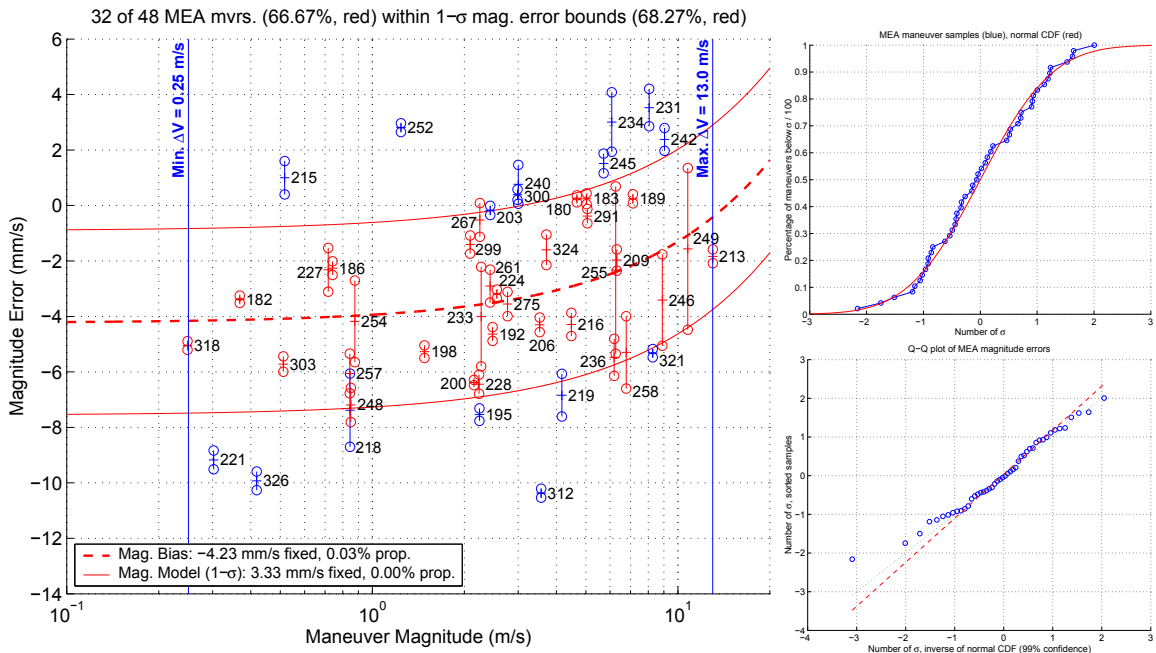
Table 1 lists the main engine and RCS maneuver execution-error model updates. The 2012-1 main engine model was developed from an analysis of 48 main engine maneuvers following propulsion’s January 2009 fuel-side repressurization through June 2012 (OTMs 180–326) and is described in the following section and documented in Reference 3. The 2012-1 RCS model was generated using data from 49 RCS maneuvers following the March 2009 thruster branch swap through July 2012 (OTMs 183x–328) and is discussed in a later section and recorded in Reference 6.

MAIN ENGINE EXECUTION-ERROR MODELING: 2012-1 STUDY

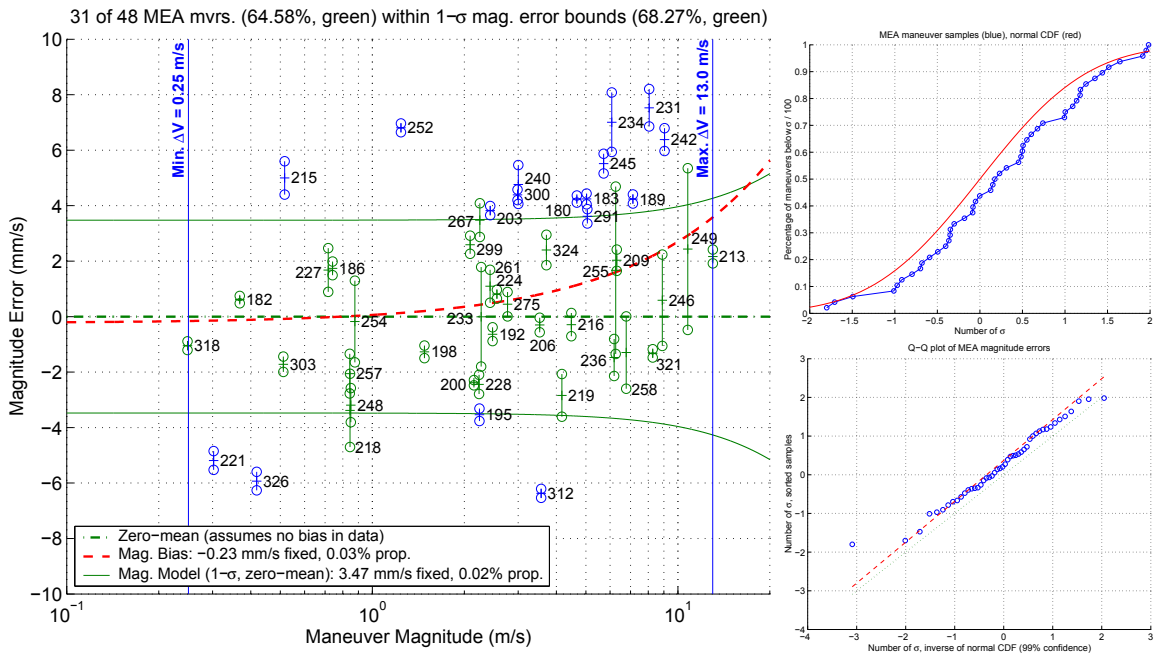
The 2012-1 main engine model represents the execution errors seen with main engine burns following Cassini’s last fuel-side repressurization in January 2009. A -3 mm/s bias in fixed magnitude was seen with the 2008-01 execution-error analysis⁹ of maneuvers performed prior to the repressurization and corrected with a change to the tail-off impulse parameter in April 2009. Similarly, the -4 mm/s fixed-magnitude bias identified in this study was effectively removed from future main engine executions via a flight software patch to the tail-off impulse parameter in July 2012.

2012-1 Main Engine Magnitude-Error Analysis (OTMs 180–326)

Figure 1 contains plots of magnitude error as a function of maneuver magnitude for the 48 main engine maneuvers considered in the 2012-1 study (within OTMs 180–326). The estimated magnitude bias and the $1-\sigma$ error bounds about the magnitude bias, given by the execution-error model, are plotted in each figure. The error bars about the maneuver data points represent the $1-\sigma$ uncertainties in the OD estimates of the magnitude errors. These uncertainties were used to weight each maneuver in the maximum-likelihood estimator. It is



(a) Estimated-Bias Model of Magnitude Errors (-4 mm/s Fixed-Mag and 0.03% Prop-Mag Biases) (b) Mag-Error CDF & Q-Q Plots for (a)



(c) Zero-Mean Model of Magnitude Errors (Removed -4 mm/s Fixed-Mag Bias, 0.03% Prop-Mag Bias Remaining) (d) Mag-Error CDF & Q-Q Plots for (c)

Figure 1: 2012-1 Study of OTMs 180–326 Main Engine Magnitude Errors

assumed with the Gates model that the magnitude errors follow a normal distribution; hence, for a one-dimensional distribution, it is expected that approximately 68% of the maneuvers will fall within the $1\text{-}\sigma$ magnitude bounds (the actual number of maneuvers within the bounds is indicated in each plot).

Figure 1a shows the magnitude errors and the estimated-bias model ($1\text{-}\sigma$ bounds and bias line, in blue) with the observed -4.2 mm/s fixed-magnitude and 0.03% proportional-magnitude biases, and Figure 1c the magnitude errors and the zero-mean model ($1\text{-}\sigma$ bounds about zero line, in green) after removing -4 mm/s of the fixed-magnitude bias via adjustments to the expected ΔV data (see Appendix C). In the estimated-bias model, it is assumed that the estimated fixed and proportional-magnitude biases are extracted. However, only the observed fixed-magnitude bias of -4 mm/s was removed. The option to also remove the computed 0.03% proportional-magnitude bias was not chosen by the Cassini Project. With a majority of the remaining main engine burns in the mission expected to fall under 10 m/s , the effect of the proportional-magnitude bias on the execution-error model was not as profound as the fixed-magnitude bias term if left in the maneuver estimates. Although the proportional-magnitude bias term remains, in Cassini operations a zero-mean model is necessary as the orbit determination filter assumes Gaussian execution errors about the maneuver ΔV s without visibility into any biases in the errors, and the predicted ΔV statistics from the maneuver software does not account for biases in the Gates model. Without the magnitude-error adjustments, the main engine maneuvers showed a tendency to underburn (37 of 48 maneuvers, 77%). Accounting for the July 2012 flight software patch to the tail-off impulse parameter in the magnitude errors yields a more even distribution of underburns (21 of 48 maneuvers, 44%) and overburns (27 of 48 maneuvers, 56%).

Figures 1b and 1d provide the cumulative distribution functions (CDFs) and quantile-quantile (Q-Q) plots for the magnitude errors for Figures 1a and 1c, respectively, where Figure 1c shows the maneuver estimates and resulting model once the -4 mm/s fixed-magnitude bias is extracted. The magnitude errors are expected to better match the CDFs and to become more linear on the Q-Q plots as the sample size grows. In Figure 1b, it can be seen that the magnitude errors from the estimated-bias model closely follow the Gaussian CDF (red curve) and the linearity of the magnitude errors in the Q-Q plot suggests that the errors are normally distributed about the computed bias. In Figure 1d, the magnitude errors from the zero-mean model are slightly offset from the Gaussian CDF (red curve) and the linearity of the magnitude errors in the Q-Q plot still holds, but with a more pronounced divergence at the tails of the distribution. This is likely a consequence of not removing the proportional-magnitude bias from the estimates, which skews the data in the zero-mean model fit.

2012-1 Main Engine Pointing-Error Analysis (OTMs 180–326)

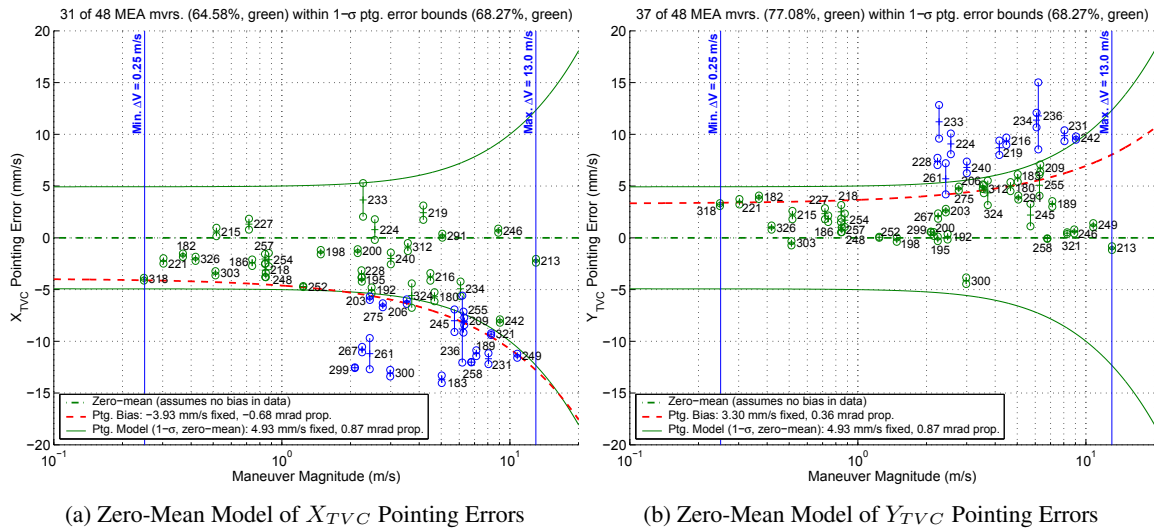


Figure 2: 2012-1 Study of OTMs 180–326 Main Engine Pointing Errors

Figure 2 illustrates the pointing error along the X_{TVC} and Y_{TVC} axes, respectively, as a function of maneuver magnitude for the main engine maneuvers. The pointing errors are assumed to follow a normal distribution per axis, therefore the Gates model $1-\sigma$ bounds are shown for the X_{TVC} and Y_{TVC} pointing errors separately. Although both fixed and proportional-pointing biases are identified, they remain in the maneuver estimates because they have not been removed through a mechanism such as a flight software change. Again, the zero-mean model is used to support the orbit determination filter and maneuver analysis software for ΔV statistics. Note, the $1-\sigma$ pointing-error bars for each maneuver which are used to weight the pointing-error data are the semi-major axis values of the pointing ellipses in the TVC plane, not the standard deviations along the respective TVC axis. Figure 2 shows that given the proportional-pointing biases of -0.7 mrad along the X_{TVC} axis and 0.4 mrad along the Y_{TVC} axis, the pointing errors of main engine maneuvers tend to be in the $-X, +Y$ quadrant of the TVC pointing plane, and range between $1-\sigma$ and $2-\sigma$ for larger main engine burns. Note, these proportional-pointing biases are not rotations about the X_{TVC} and Y_{TVC} axes. Rather, they are angular offsets in the X_{TVC} and Y_{TVC} directions. The pointing biases determined in the 2008-01 study also indicated this pointing tendency (see Table 3 in Appendix A). Without removing these proportional-pointing biases, it is expected that future maneuver engine burns will share similar pointing-error characteristics.

MAIN ENGINE EXECUTION-ERROR MODELING: JANUARY 2014 ASSESSMENT

The main engine maneuver performance following the 2012-1 model update was determined from 14 main engine burns executed from August 2012 through December 2013 (OTMs 330–366). These 14 maneuvers were performed after the July 2012 flight software patch to the tail-off impulse parameter in the magnitude errors which effectively removed the -4 mm/s fixed-magnitude bias seen in main engine burns from OTMs 180–326 in the 2012-1 study. This performance assessment shows that the 2012-1 magnitude-error model for main engine is adequate and no action is required to remove the fixed-magnitude bias, unless the proportional-magnitude bias is also removed. The assessment also reveals a pointing-error model and associated biases similar to the 2012-1 study.

January 2014 Main Engine Magnitude-Error Assessment (OTMs 330–366)

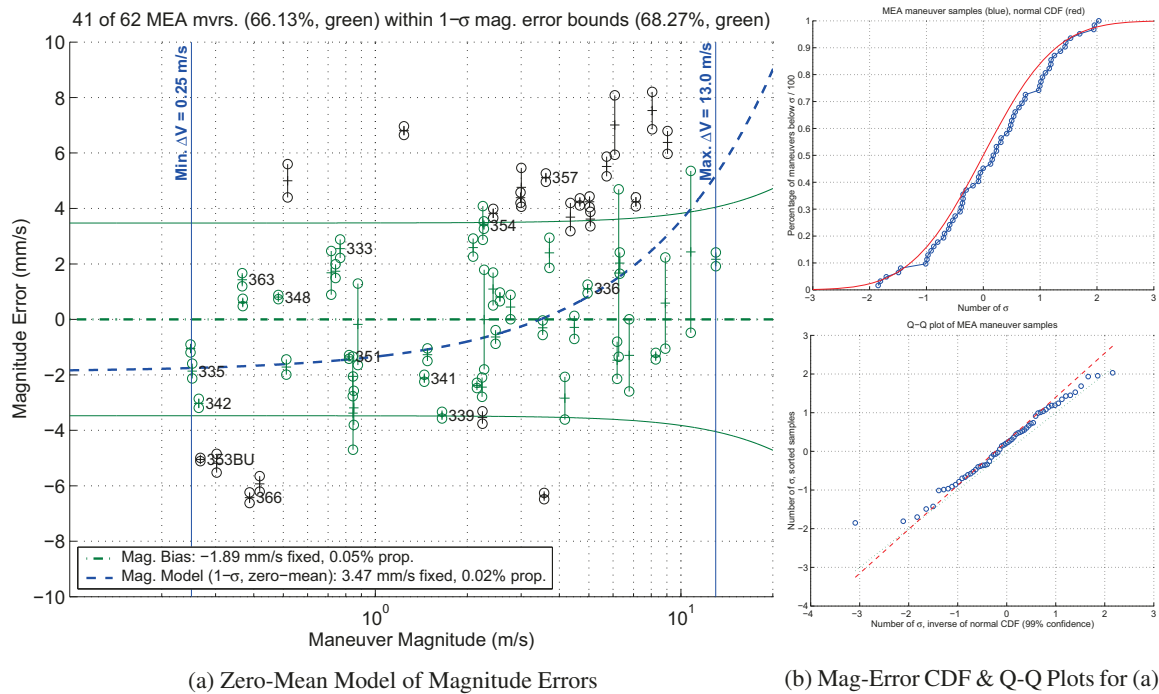


Figure 3: Jan. 2014 Study of OTMs 180–366 Main Engine Magnitude Errors (OTMs 330-366 Labeled)

As seen in Figure 3, the magnitude-error uncertainties of the 2012-1 main engine model hold well given the performance of 14 main engine burns executed from August 2012 through December 2013 (OTMs 330–366). This also implies that the -4 mm/s fixed-magnitude bias was correctly identified and that the flight software patch to the main engine tail-off impulse parameter was effective in removing this bias. One benefit of taking out the fixed-magnitude bias is that the magnitude errors will be more equally distributed about zero. Most main engine magnitude errors can now be expected to fall within ± 4 mm/s, which was the case for all main engine maneuvers considered in this performance study.

January 2014 Main Engine Pointing-Error Assessment (OTMs 330–366)

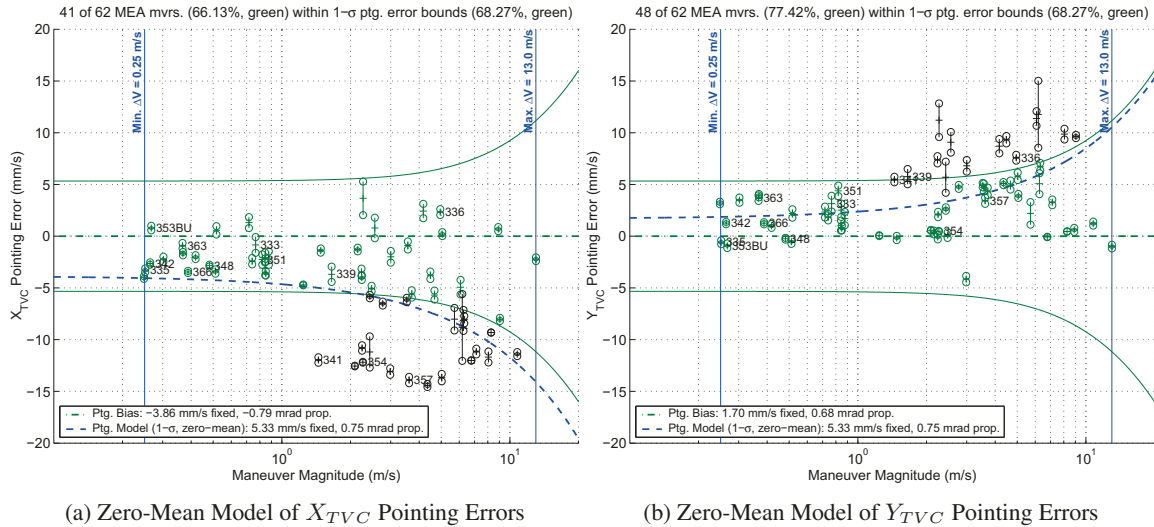


Figure 4: Jan. 2014 Study of OTMs 180–366 Main Engine Pointing Errors (OTMs 330-366 Labeled)

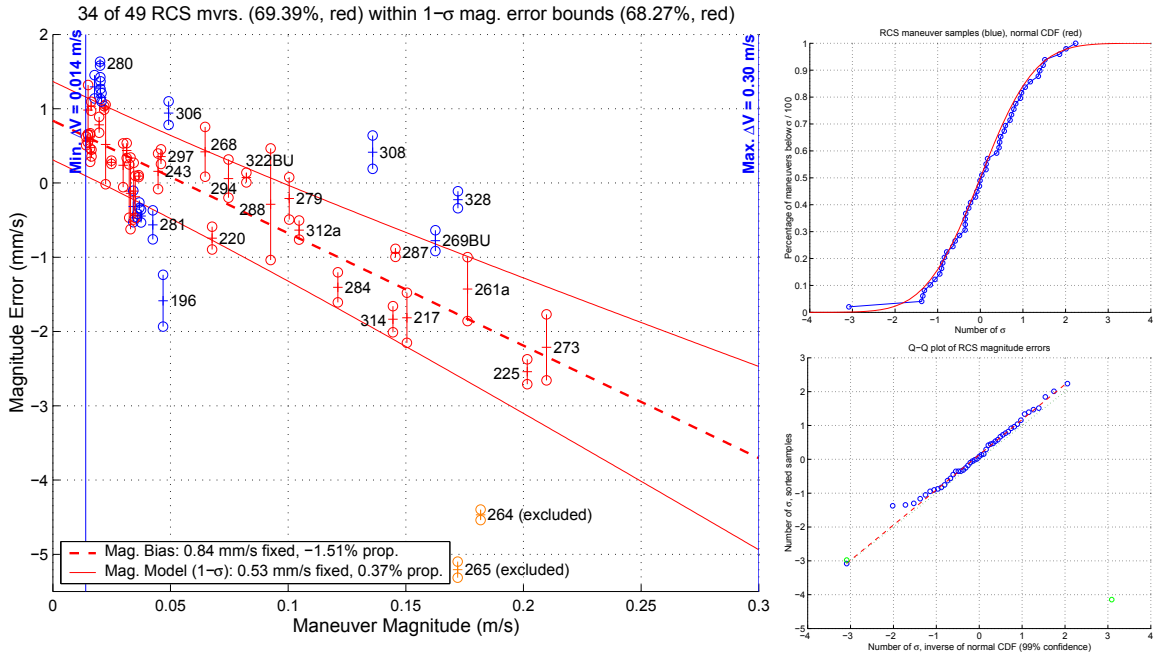
Figure 4 illustrates the pointing error along the X_{TVC} and Y_{TVC} axes, respectively, as a function of maneuver magnitude for the main engine maneuvers. Because the proportional-pointing biases in the main engine execution errors were not removed with the 2012-1 model update, the maneuvers continue to share similar pointing-error characteristics as expected.

RCS EXECUTION-ERROR MODELING: 2012-1 STUDY

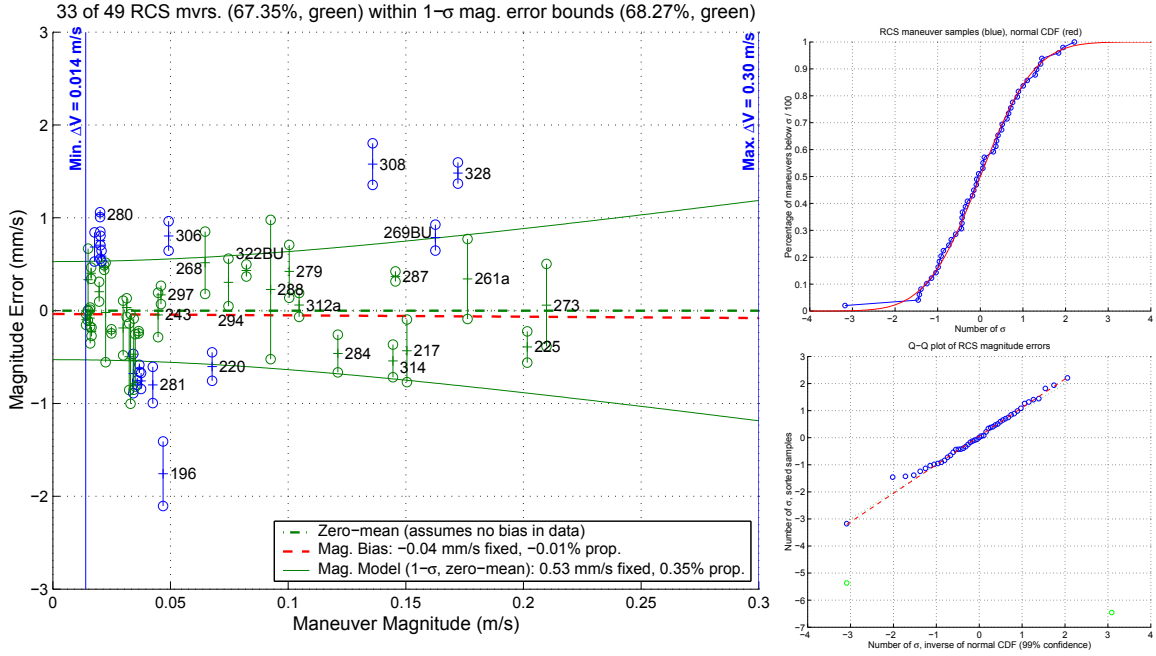
The 2012-1 RCS model is the first to characterize the execution errors seen with RCS maneuvers performed via the redundant B-branch thrusters (set of eight thrusters), the main A-branch thrusters (identical set of eight thrusters) relegated to backup in March 2009 because of a marked degradation in performance. The detected proportional-magnitude bias was removed by Propulsion via a -1.5% change to the RCS thrust adjustment factor.¹⁰ The fixed-magnitude bias was taken out by Navigation by adding 0.8 mm/s to the 5.0 mm/s deadband-tightening ΔV which was specified in the RCS maneuver designs. This updated value of 5.8 mm/s serves as both a correction for the average deadband-tightening ΔV seen by Navigation and the fixed-magnitude bias observed in RCS maneuver executions.

2012-1 RCS Magnitude-Error Analysis (OTMs 183x–328)

Figure 5 provides plots of magnitude error versus maneuver magnitude for the RCS burns examined in the 2012-1 study (see main engine execution-error analysis section for an explanation of these plots). Figure 5a displays the magnitude errors and the magnitude-error model/bias lines with the observed -1.5% proportional-magnitude and $+0.8$ mm/s fixed-magnitude biases. Figure 5c shows the magnitude errors and



(a) Estimated-Bias Model of Magnitude Errors (-1.5% Prop-Mag and +0.8 mm/s Fixed-Mag Biases) (b) Mag-Error CDF & Q-Q Plots for (a)



(c) Zero-Mean Model of Magnitude Errors (Removed-1.5% Prop-Mag and +0.8 mm/s Fixed-Mag Biases) (d) Mag-Error CDF & Q-Q Plots for (c)

Figure 5: 2012-1 Study of OTMs 183x-328 RCS B-Branch Magnitude Errors

the zero-mean magnitude-error model lines after extracting both the fixed and proportional-magnitude biases, $+0.8$ mm/s and -1.5% , respectively, through modifications to the expected ΔV data. Without the magnitude-error adjustments, the RCS maneuvers showed a slight tendency to overburn (26 of 49 maneuvers, 53%). Accounting for the September 2012 thrust factor adjustment and the $+0.8$ mm/s fixed-magnitude correction results in a more even distribution of overburns (24 of 49 maneuvers, 49%) and underburns (25 of 49 maneuvers, 51%).

2012-1 RCS Pointing-Error Analysis (OTMs 183x–328)

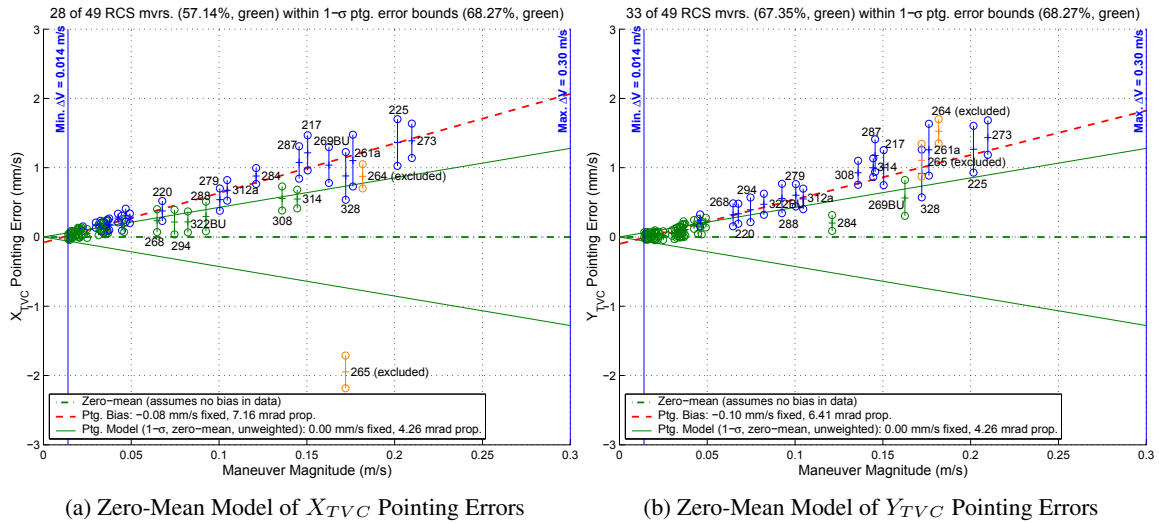


Figure 6: 2012-1 Study of OTMs 183x–328 RCS B-Branch Pointing Errors

Figure 6 illustrates the pointing error along the X_{TVC} and Y_{TVC} axes, respectively, as a function of maneuver magnitude for the RCS maneuvers. The zero-mean pointing-error model lines are plotted because both fixed- and proportional-pointing biases remain in the maneuver data. The pointing errors are assumed to follow a normal distribution per axis, therefore the Gates model $1-\sigma$ bounds are shown for the X_{TVC} and Y_{TVC} pointing errors separately. Again, this type of model is necessary because the orbit determination filter does not have visibility into any underlying biases in the pointing errors.

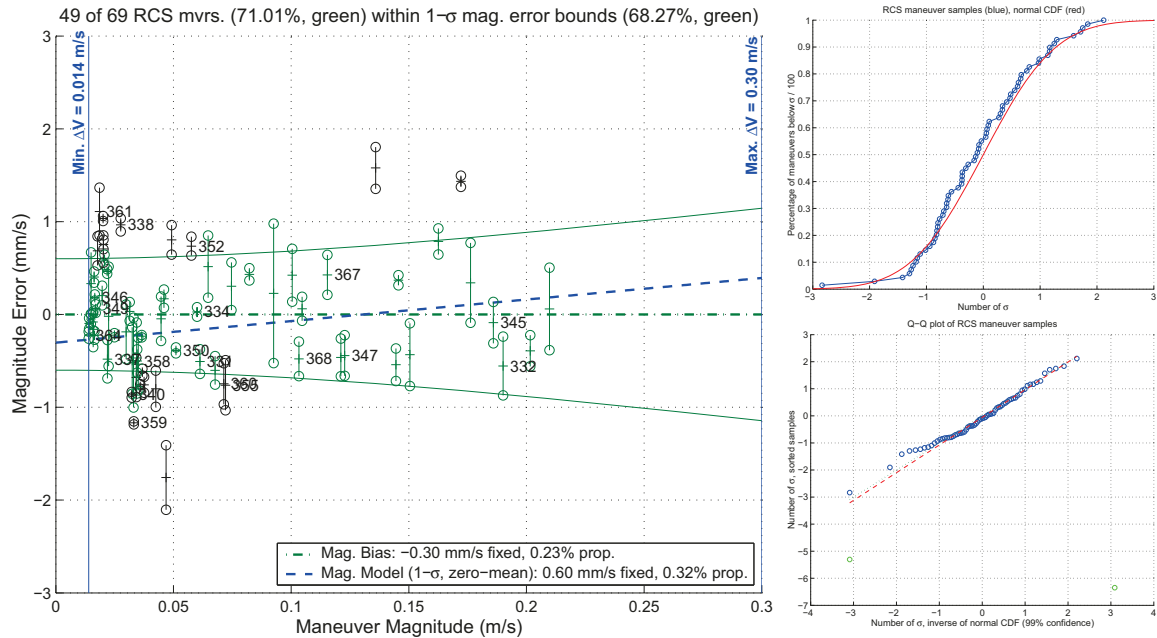
The weighted estimation of the proportional-pointing error parameter yielded a value of 3.4 mrad, as opposed to an unweighted estimation of 4.3 mrad. The unweighted model for the proportional-pointing error parameter was chosen (rounded to 4.5 mrad), see Figure 6, to remove the effect that the tight uncertainties on the smaller RCS burns had on the estimation of the proportional-pointing standard deviation, an effect that favored the smaller burns and did not well represent the larger burns. With the weighted model, nearly 68% of the maneuvers fell within the $1-\sigma$ pointing-error bounds for pointing errors along the Y_{TVC} axis (this is the limiting case because only 57% of maneuvers fall within the bounds for the pointing errors along the X_{TVC} axis). Because 68% of maneuvers fall within the $1-\sigma$ bounds, this explains why the pointing-error biases on both axes are not contained within the computed standard deviations of the pointing-error model.

Figure 6 shows that given the proportional-pointing biases of 7.2 mrad along the X_{TVC} axis and 6.4 mrad along the Y_{TVC} axis, the pointing errors of RCS maneuvers tend to be in the $+X$, $+Y$ quadrant of the TVC pointing plane, and range between $+1-\sigma$ and $+2-\sigma$ for larger RCS burns. Like with main engine maneuvers, these proportional-pointing biases are not rotations about the X_{TVC} and Y_{TVC} axes, but angular offsets in the X_{TVC} and Y_{TVC} directions. Without the removal of these proportional-pointing biases, it is expected that future RCS burns performed on B-branch thrusters will continue to have similar pointing-error characteristics.

RCS EXECUTION-ERROR MODELING: JANUARY 2014 ASSESSMENT

The RCS maneuver performance following the 2012-1 model update was determined from 20 RCS burns executed from September 2012 through January 2014 (OTMs 331–368). These 20 maneuvers were performed with the observed magnitude-error biases seen in the 2012-1 study removed within the maneuver design process. This performance assessment shows that the 2012-1 magnitude-error model for RCS is adequate and no action is required to remove the magnitude biases. The assessment also reveals a pointing-error model and associated biases similar to the 2012-1 study.

January 2014 RCS Magnitude-Error Assessment (OTMs 331–368)



(a) Zero-Mean Model of Magnitude Errors

(b) Mag-Error CDF & Q-Q Plots for (a)

Figure 7: Jan. 2014 Study of OTMs 183x–368 RCS B-Branch Magnitude Errors (OTMs 331–368 Labeled)

As seen in Figure 7, the magnitude-error uncertainties of the 2012-1 RCS model agree with the performance of 20 RCS maneuvers from September 2012 to January 2014 (OTMs 331–368). This also suggests that the fixed and proportional-magnitude biases were correctly recognized and that the changes to the RCS design process were sufficient in removing these biases. An advantage of extracting the magnitude biases is that the magnitude errors should be equally distributed about zero. A majority of RCS magnitude errors can now be expected to fall within ± 1 mm/s, which was the case for all RCS burns evaluated in this study.

January 2014 RCS Pointing-Error Assessment (OTMs 331–368)

Figure 8 illustrates the pointing error along the $X_{TV C}$ and $Y_{TV C}$ axes, respectively, as a function of maneuver magnitude for the RCS maneuvers. Because the proportional-pointing biases in the RCS execution errors were not removed with the 2012-1 model update, the maneuvers continue to share similar pointing-error characteristics as expected.

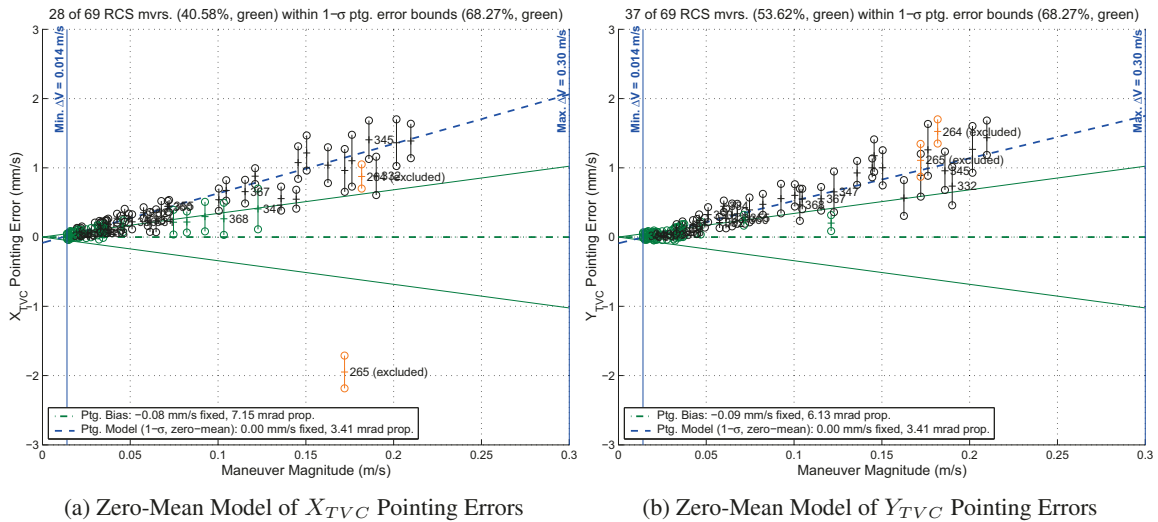


Figure 8: Jan. 2014 Study of OTMs 183x–368 RCS B-Branch Pointing Errors (OTMs 331–368 Labeled)

METHODS FOR DEVELOPING EXECUTION-ERROR MODELS

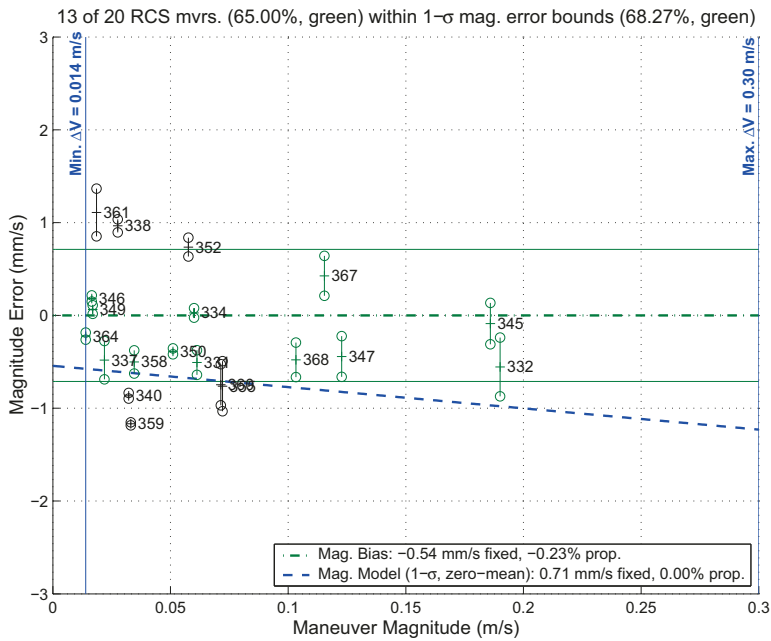
It is recommended that the following are considered when developing an execution-error model to describe the performance of a propulsion system:

1. A sufficient maneuver data set, both in size and range, should be used in the determination of the model and associated biases.
2. Outliers in the data set should be identified and investigated individually. In some circumstances, an identified outlier may be excluded from the data set.
3. If possible, identified biases should be removed either through a flight parameter change or within the maneuver design process.
4. If changes were made to the maneuver executions to remove identified biases, maneuver data prior to these changes should be adjusted to account for these modifications if considered in future analysis. Appendix C details how prior data for Cassini’s main engine and RCS maneuvers are adjusted.

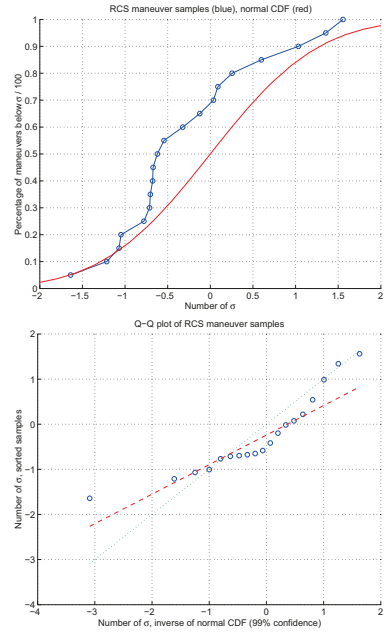
This section presents examples of the first two considerations through analyzing Cassini maneuver data. Lessons learned in generating plots of the magnitude and pointing errors are also discussed.

Determining Sufficiency in a Maneuver Data Set

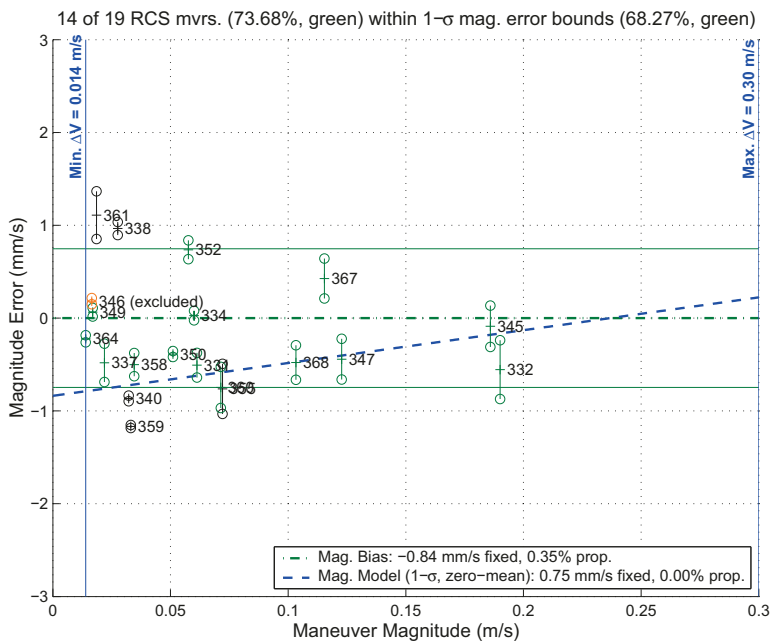
Developing a representative execution-error model requires a sufficient data set, in both amount and range. This data set may take some time to grow, and later evaluations may reveal that the data set is still not complete. One indication that a data set is sufficient is that the removal of one maneuver does not greatly alter the nature of the model or computed biases. For the example shown in Figure 9, the removal of OTM-346 caused both the fixed and proportional magnitude bias terms to change drastically. OTM-346 is one of only three maneuvers in the smallest ΔV range. Because this point is well determined, it has a great influence in the estimation of the fixed-magnitude bias term. When accounting for all B-branch RCS maneuvers performed in this ΔV range, the removal of OTM-346 does not influence the bias determination, indicating that the entire data set of nearly 70 maneuvers is sufficient.



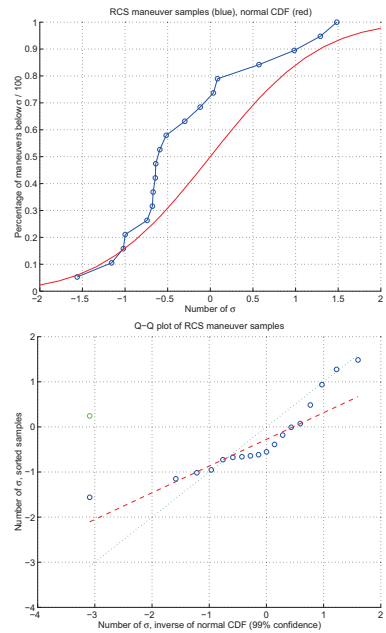
(a) Zero-Mean Model of Magnitude Errors (with OTM-346)



(b) Mag-Error CDF & Q-Q Plots for (a)



(c) Zero-Mean Model of Magnitude Errors (Excluding OTM-346)



(d) Mag-Error CDF & Q-Q Plots for (c)

Figure 9: Jan. 2014 Study of OTMs 331–368 RCS Magnitude Errors

Identifying and Excluding Outliers from a Maneuver Data Set

The determination of outliers in a given maneuver data set can be challenging. Once a maneuver sample is identified as a possible outlier in either magnitude or pointing, the circumstances surrounding that particular maneuver should also be investigated. This section presents a few examples of identified outliers that were excluded from the 2012-1 RCS study.

OTM-264 was an RCS maneuver excluded from the 2012-1 RCS analysis for its significantly smaller deadband-tightening ΔV as compared to other RCS maneuvers. The estimated deadband-tightening ΔV of 1.5 mm/s for this RCS burn was well below the predicted value of 5 mm/s, accounting for an extra 3.5 mm/s in underburning. This outlier in magnitude error can be seen in Figure 5a.

OTM-265, also an RCS maneuver, was found to be an outlier in both magnitude and pointing (see Figures 5a and 8a). Due to a safing event on November 2, 2010,¹¹ the spacecraft was under RCS control for all turns, which included OTM-265. The safing event had also reset the prime flight computer (resetting the pulse adjuster attitude error gain to zero), in turn causing noticeable changes to both magnitude and pointing. Once the attitude control integrators were re-established via ground command, subsequent RCS burns returned to expected accuracies (see Reference 12).

Visualization of Execution Errors

In conjunction with tables, viewing the execution errors in plots such as magnitude error as a function maneuver magnitude can be quite useful in the analysis process. However, determining how to plot the execution errors brings its own set of challenges. This section offers some advice for making these types of plots, lessons learned from processing Cassini maneuver data over the years.

For example, a plot containing the magnitude errors from a large set of maneuvers may become cluttered and difficult to label. A semi-logarithmic scale helps to reveal details on a plot with a large range of maneuver magnitude (see Figures 1-4).

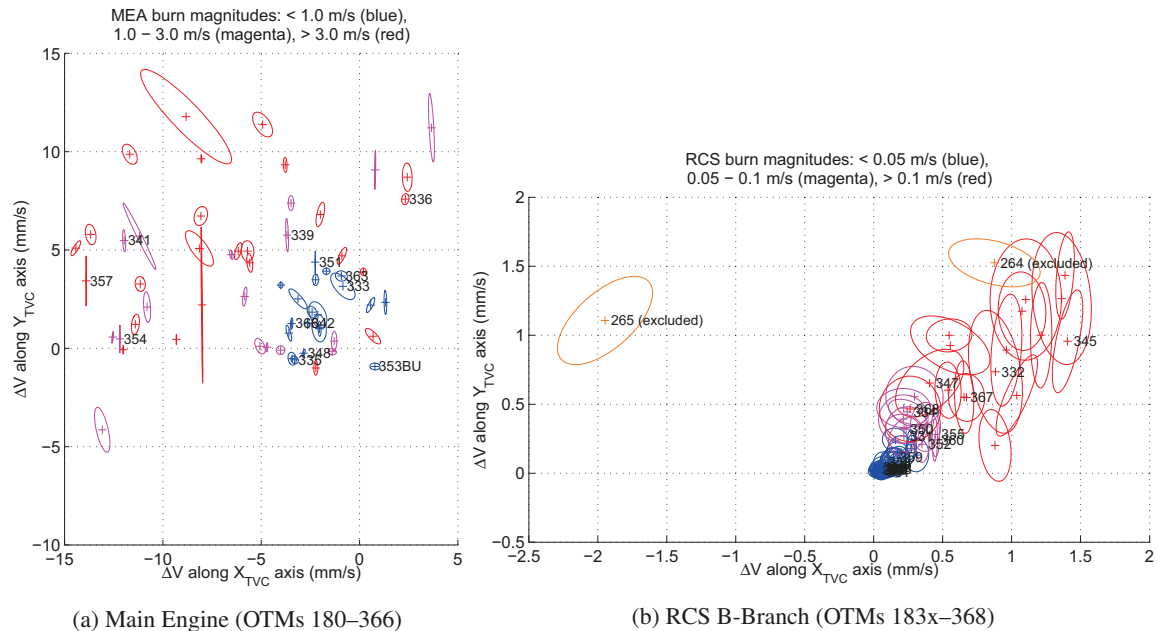


Figure 10: Main Engine and RCS Pointing Errors in TVC Pointing Plane

Pointing errors are particularly difficult to depict on a plot. Figure 10 shows the main engine and RCS pointing errors mapped to the thrust-vector-control (TVC) pointing plane. To add the dimension of maneuver magnitude, ellipses have been color-coded to display their relationship with maneuver magnitude.

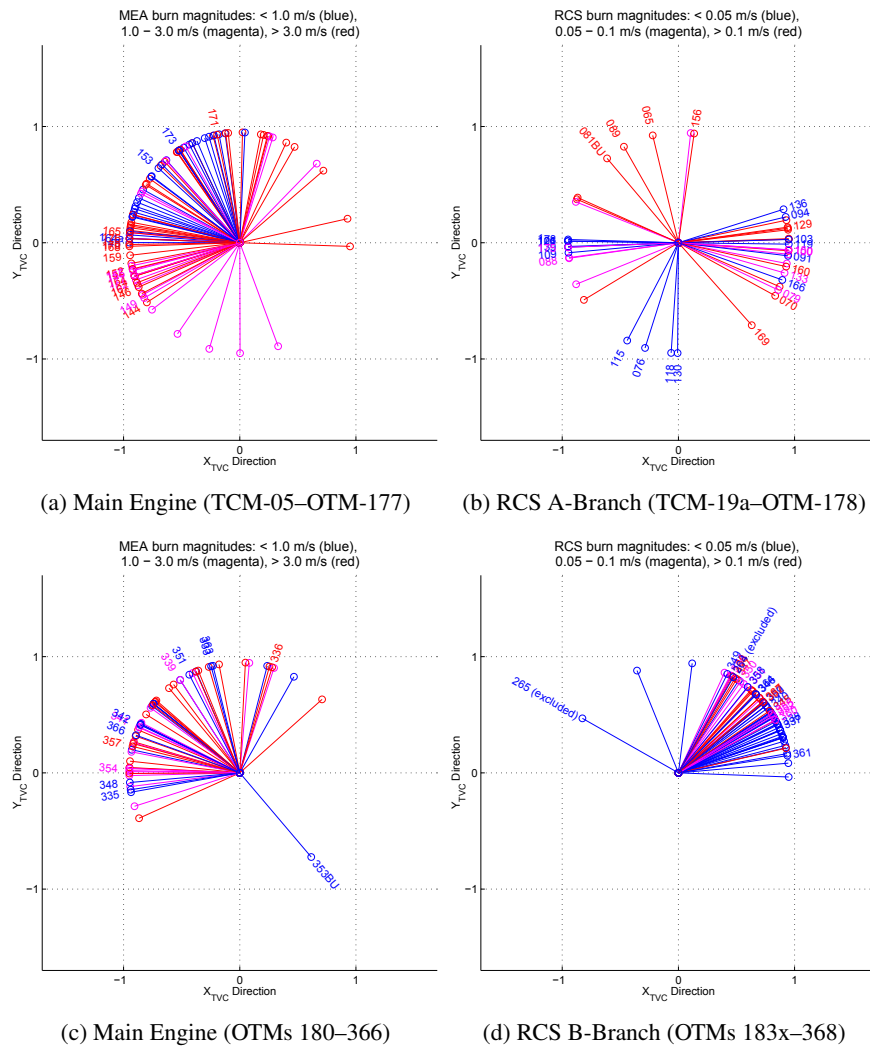


Figure 11: Main Engine and RCS Pointing-Error Directions

The direction of the pointing errors can be illustrated in plots such as Figure 11. Again, the maneuver magnitudes can be displayed using color coding. These types of plots help show tendencies in the pointing. If the pointing is unbiased, the directions from the given maneuver samples should be uniformly distributed across 360° . As seen in Figures 11a and 11c, the majority of the main engine burns are in the $-X, +Y$ quadrant of the TVC plane. Similarly, as shown in Figure 11d, almost all RCS maneuvers performed on B-branch are contained in the $+X, +Y$ quadrant. Only the RCS maneuvers on A-branch have a more diverse pointing spread about 360° (see Figure 11b).

Both the TVC pointing errors and pointing-error direction plots need to be considered to understand the nature of each individual maneuver sample. For example, the main engine maneuver OTM-353 BU, as denoted in Figure 11a, immediately jumps out as an outlier in pointing direction as compared to the other maneuvers. When viewed with Figure 10a, it is seen that OTM-353 BU had a small pointing error nearly centered at (0,0). The pointing error ellipse can move to the other side of (0,0) by a small amount to be in family with the majority of the maneuvers. Because of this, OTM-353 BU would not be considered an outlier in pointing. On the other hand, the RCS maneuver OTM-265, as shown in Figures 10b and 11b, was found to be an outlier in both magnitude and pointing (see next section). Figure 10b clearly shows that the pointing error was not in family with the rest of the RCS maneuvers.

DETECTING DEGRADATION OR SIGNIFICANT CHANGES IN MANEUVER PERFORMANCE

In prior sections, it was shown how representative models of the maneuver execution errors can effectively be used to assess maneuver performance. These same models can also be used to flag large outliers in the data, which may signify either a large change in the way the maneuver was executed or indicate a possible degradation of the engine or thruster. In magnitude, this would point to a change or degradation in propulsion. Likewise, in pointing, this would indicate a change or degradation in attitude control. By comparing each maneuver sample to how the execution-error model was prior to adding the sample, a method for detecting outliers can be established:

1. Maneuver is an outlier using previous execution-error model which does not include the maneuver.
2. Execution-error model or biases change significantly when the maneuver is introduced.
3. Following maneuvers are also outliers and execution-error model changes significantly. This is the key criterion for detecting degradation.

The following example presents an actual degradation case with two of Cassini's A-branch set of eight RCS thrusters, requiring a swap to the redundant B-branch set of thrusters.

Example: Cassini RCS A-Branch Thruster Degradation in 2008

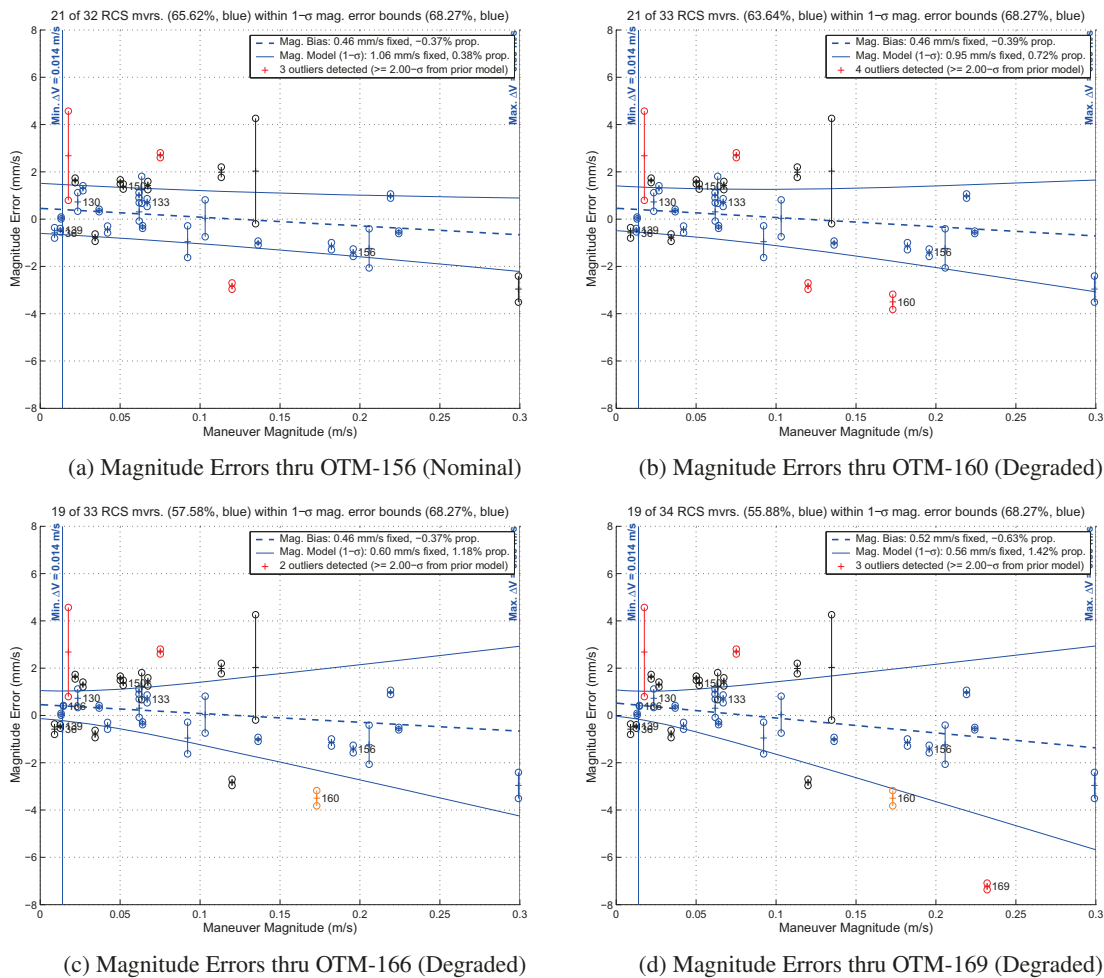


Figure 12: RCS Estimated-Bias Models for Maneuvers on A-Branch Thrusters (TCM-19a–OTM-169)

In late 2008, the degradation of two RCS thrusters on the A-branch became apparent from a Navigation perspective by the multi- σ under-performance of OTM-160 and OTM-169. Figure 12 shows how adding OTM-160 and OTM-169 significantly alters the RCS magnitude-error model. In this example, a maneuver is flagged as an outlier if it is over $2\text{-}\sigma$, using the prior magnitude-error model as the metric. Note, three older maneuvers in the data set were flagged as outliers, but are not considered outliers because it is expected that there will be multi- σ samples in the distribution. Figure 12a gives the execution-error model prior to the RCS degradation on the A-branch (up to OTM-156). The computed execution-error model was close to the nominal 2008-01 RCS model. Figure 12b shows the first sign of degradation with the A-branch thrusters with an RCS maneuver (OTM-160). The model notably changes with the introduction of the multi- σ under-burning of OTM-160. Figure 12c adds OTM-166 to the data set, however this maneuver is not flagged as an outlier. OTM-166 was degraded in its performance, but this is not apparent in the execution-error modeling due to its small ΔV size. Finally, Figure 12d provides the execution-error model when OTM-169 is included in the maneuver samples. OTM-169 was executed as a large RCS burn with a ΔV of 0.23 m/s, the final approach maneuver targeting Titan-46 (part of a double flyby with Enceladus-6). The large magnitude error of this maneuver resulted in a nearly 10 km miss of the low 1100 km Titan flyby and a downstream cost of over 7 m/s. This sub-par performance helped lead to a swap to the redundant B-branch thrusters in March 2009.^{4,5}

CONCLUSIONS

Analyzing the execution errors of the Cassini spacecraft's main engine and RCS maneuvers has proven advantageous for Cassini Navigation, and adjusting the maneuver performance based on this Navigation analysis has benefited the entire Cassini Mission with more accurate maneuvers. Even with over 15 years of in-flight maneuver data to study, there is still much to learn about the execution errors of Cassini's propulsion systems. Fortunately, what has been learned can be used to help improve the performance of future Cassini maneuvers.

The execution-error modeling methods and lessons learned presented in this paper can also assist in the evaluation and characterization of other spacecraft's maneuver performance. For example, a representative execution-error model can be used to detect degraded performance or a large change in an engine or thruster's maneuver executions. This type of analysis would have confirmed the degraded performance of Cassini's RCS thrusters on A-branch in 2008, and it is now currently utilized on Cassini for monitoring the maneuver performance of the RCS B-branch thrusters.

With several years left in the Cassini Solstice Mission, the improvements to the execution-error models and maneuver executions discussed in this paper will continue to be verified as more maneuver data is processed and further updates will be implemented if necessary.

APPENDIX A: HISTORY OF EXECUTION-ERROR MODELS

Throughout the Cassini Mission there have been several main engine and RCS execution-error model updates, as seen in Table 2. They continue to be in the form of the Gates model,² which accounts for magnitude and pointing errors. In 2000, the MEA component of the pre-launch model was updated via an analysis of seven main engine maneuvers performed during the first two years of the interplanetary cruise. The resulting 2000 model¹³ was used for maneuvers from April 2000 during cruise to February 2006 into the Saturn tour.

The 2006-01 model was used from March 2006, starting with OTM-053, to August 2007, ending with OTM-124. Besides reducing the MEA magnitude and proportional error parameters and the RCS magnitude error parameters, this model introduced a few changes in spacecraft operations. The computed RCS proportional-magnitude bias was removed by reducing the predicted thrust level by 1.5% starting with the design of OTM-047. Also, beginning with OTM-069, the MEA proportional-magnitude bias seen in the

Table 2: History of Execution-Error Models(a) Main Engine Execution-Error Models (1- σ)

		Pre-Launch	2000	2006-01, 2007-01	2007-02	2008-01	2012-1
Magnitude	Proportional (%)	0.35	0.2	0.04	0.02	0	0.02
	Fixed (mm/s)	10.0	10.0	6.5	5.0	4.5	3.5
Pointing (per axis)	Proportional (mrad)	10.0	3.5	1.0	0.6	1.1	1.0
	Fixed (mm/s)	17.5	17.5	4.5	3.0	3.0	5.0
<i>Main engine burns investigated</i>		N/A	TCMs 05-13	TCM-05- OTM-042	TCM-05- OTM-128	TCM-05- OTM-168	OTMs 180-326
<i>No. of main engine burns (excluded)</i>		N/A	7 (1)	38 (2)	61 (10)	85 (9)	48 (0)
<i>Valid for main engine burns</i>		All	All	All	All	≤ 25 m/s	≤ 13 m/s
<i>Model first implemented</i>		TCM-01 (10/1997)	TCM-14 (4/2000)	OTM-056 (3/2006)	OTM-144 (2/2008)	OTM-192 (4/2009)	OTM-330 (8/2012)

(b) RCS Execution-Error Models (1- σ)

		Pre-Launch, 2000	2006-01	2007-01	2007-02, 2008-01	2012-1
Magnitude	Proportional (%)	2.0	0.7	0.7	0.4	0.4
	Fixed (mm/s)	3.5	0.9	0.9	1.0	0.5
Pointing (per axis)	Proportional (mrad)	12.0	12.0	12.0	9.0	4.5
	Fixed (mm/s)	3.5	3.5	0	0	0
<i>RCS maneuvers investigated</i>		N/A	TCM-19a- OTM-044	N/A	TCM-19a- OTM-129	OTMs 183x-325
<i>No. of RCS maneuvers (excluded)</i>		N/A	11 (2)	N/A	26 (11)	49 (2)
<i>Valid for RCS maneuvers</i>		All A-branch & B-branch	All A-branch	All A-branch	≤ 0.3 m/s (A-branch)	≤ 0.3 m/s (B-branch)
<i>Model first implemented</i>		TCM-02 (10/1997)	OTM-053 (3/2006)	OTM-127 (9/2007)	OTM-148 (2/2008)	OTM-331 (9/2012)

Table 3: History of Execution-Error Biases

		<i>Main Engine Biases</i>				<i>RCS Biases</i>		
		2006-01, 2007-01	2007-02	2008-01	2012-1	2006-01, 2007-01	2007-02, 2008-01	2012-1
Magnitude	Proportional (%)	0.06 (0)	-0.02	-0.02 (0)	0.03	1.5 (0)	-0.4	-1.5 (0)
	Fixed (mm/s)	-4.5	-3.2	-3.1 (-0.1)	-4.2 (-0.2)	0	0.5	0.8 (0)
Pointing (X_{TVC} axis)	Proportional (mrad)	0.3	-0.7	-1.1	-0.7	7.5	5.0	7.2
	Fixed (mm/s)	-9.0	-3.4	-2.3	-3.9	0.8	0.3	-0.1
Pointing (Y_{TVC} axis)	Proportional (mrad)	1.5	0.7	0.5	0.4	-4.5	-1.2	6.4
	Fixed (mm/s)	-3.0	1.2	1.2	3.3	3.5	0	-0.1

2006-01 study was removed by increasing the MEA accelerometer scale factor by 0.06%.¹⁴ These extracted biases are indicated in Table 3. The 2006-01 RCS model as listed in Table 2b is not directly from the maneuver estimation process. There were not enough RCS maneuvers in the analysis to confidently use the RCS pointing-error model, so those terms were carried over from the 2000 model.

The 2007-01 model was used from September 2007 with OTM-125 through January 2008 with OTM-143. Based on the 2006-01 model, it reduced the RCS fixed-pointing error standard deviation from 3.5 mm/s to 0 mm/s as RCS OTM turns use the Reaction Wheel Assembly (RWA), which do not produce a turn ΔV . The 2007-01 model was meant to be an interim model until the next execution-error analysis.¹⁵

The 2007-02 model is based on the analysis of maneuvers from interplanetary cruise through September 2007 with OTM-129. This model was used from February 2008 through July 2012.¹ No changes were made to extract observed execution-error biases. This was the last update to the execution-error model of RCS maneuvers on A-branch thrusters.

The 2008-01 model was an update to the main engine execution-error model, developed from a data set of reconstructed main engine maneuvers from cruise through October 2008.⁹ Both main engine magnitude-error biases identified in the 2008-01 study were removed via a change to the accelerometer scale factor by -0.02% and to the tail-off impulse parameter by -3 mm/s. The 2008-01 RCS model is the same as the 2007-02 model.

The 2012-1 model is the latest execution-error model that has been in use since August 2012. The 2012-1 main engine model was developed from an analysis of 48 main engine maneuvers following propulsion's January 2009 fuel-side repressurization through June 2012 (OTMs 180–326) and is described in this paper.³ The 2012-1 RCS model was generated using data from 49 RCS maneuvers following the March 2009 thruster branch swap through July 2012 (OTMs 183x–328) and is discussed in this paper.⁶ The -4 mm/s fixed-magnitude bias identified for main engine burns was effectively removed through a flight software patch to the tail-off impulse parameter in July 2012. The proportional-magnitude bias was extracted by Propulsion via a -1.5% change to the RCS thrust adjustment factor.¹⁰ The fixed-magnitude bias was removed by Navigation by adding 0.8 mm/s to the estimated 5.0 mm/s deadband-tightening ΔV specified for RCS maneuver designs. This 5.8 mm/s value serves as both a correction for the average deadband-tightening ΔV estimated by Navigation and the fixed-magnitude bias observed in RCS maneuver executions.

APPENDIX B: MAXIMUM-LIKELIHOOD ESTIMATION

The Gates-model parameters are determined herein with maximum-likelihood estimation.¹⁶ In a coordinate system whose x axis is parallel to the desired ΔV , the Gates model gives the following covariance:

$$P_{\text{Gates}} = \begin{pmatrix} \sigma_1^2 + v^2\sigma_2^2 & 0 & 0 \\ 0 & \sigma_3^2 + v^2\sigma_4^2 & 0 \\ 0 & 0 & \sigma_3^2 + v^2\sigma_4^2 \end{pmatrix}, \quad (1)$$

where v is the magnitude of the maneuver ΔV , σ_1 and σ_2 are the fixed and proportional Gates-model parameters for magnitude, and σ_3 and σ_4 are the fixed and proportional Gates-model parameters for pointing. For any given maneuver, the Gates model is Gaussian $N(0, P_{\text{Gates}})$, but for a set of maneuvers with different ΔV magnitudes, it is not Gaussian because the standard deviation is a function of v . As a result, the standard deviation of the execution-error model is not simply the standard deviation of the samples; it must be obtained using a method like maximum-likelihood estimation. The procedure for this method is to derive a likelihood expression as a function of the model parameters and then maximize the likelihood of the given observations.

First, the probability density function (pdf) for the magnitude error is

$$f_m(x, v, \sigma_1, \sigma_2) = [2\pi(\sigma_1^2 + v^2\sigma_2^2)]^{-1/2} \exp \left[-\frac{1}{2} \frac{(x - \mu_m)^2}{\sigma_1^2 + v^2\sigma_2^2} \right], \quad (2)$$

where x is the magnitude error, $\mu_m = \mu_1 + v\mu_2$ is the mean magnitude error, μ_1 is the fixed-magnitude error bias, and μ_2 is the proportional-magnitude error bias. Then the likelihood function for magnitude errors, L_m , is defined as the product of evaluations of f_m for each measurement:

$$L_m(\sigma_1, \sigma_2) = \prod_{i=1}^N f_m(x_i, v_i, \sigma_1, \sigma_2). \quad (3)$$

Likewise, for the pointing error, a two-dimensional vector, the pdf is

$$f_p(\vec{x}, v, \sigma_3, \sigma_4) = \left[\sqrt{2\pi}(\sigma_3^2 + v^2\sigma_4^2) \right]^{-1} \exp \left[-\frac{1}{2} \frac{|\vec{x} - \vec{\mu}_p|^2}{\sigma_3^2 + v^2\sigma_4^2} \right], \quad (4)$$

where \vec{x} is the pointing error vector in units of velocity, $\vec{\mu}_p = \vec{\mu}_3 + v\vec{\mu}_4$ is the mean pointing error, $\vec{\mu}_3$ is the fixed-pointing error bias, and $\vec{\mu}_4$ is the proportional-pointing error bias. The likelihood function for pointing errors, L_p , is then defined as follows:

$$L_p(\sigma_3, \sigma_4) = \prod_{i=1}^N f_p(\vec{x}_i, v_i, \sigma_3, \sigma_4). \quad (5)$$

A weighted maximum-likelihood approach is constructed by raising each term in the likelihood function to a power. For the magnitude errors, the exponent is the inverse of the reconstruction's 1- σ uncertainty. For pointing errors, the uncertainty is two-dimensional, so the inverse of the standard deviation of the error along the pointing-error direction is used. The Gates-model parameters for magnitude errors are found by maximizing L_m ; likewise for pointing errors L_p . Here we maximize the natural logarithms of L_m and L_p , rather than the likelihood functions directly (adding numbers instead of multiplying numbers). Because the natural logarithm is a monotonically increasing function, the solutions will be the same.¹⁶

Based on the form of Eqs. 2 and 4, only two measurements are required to determine the parameters (solving two unknowns requires two equations). It follows that with more measurements, more accurate estimates will be produced.

APPENDIX C: PROCESSING OF MANEUVER DATA

In assembling the maneuver execution-error data that will be fitted, it may seem appropriate to just simply subtract the reconstructed ΔV from the design ΔV in an inertial coordinate system like EME2000 to obtain the maneuver execution error. However, this approach does not provide insight into the source of the error, may not provide proper bias estimates, and may not be consistent with the orbit determination.

One issue is there are events associated with each maneuver that, although they may not be part of the maneuver ΔV design, cannot be cleanly separated out in the orbit determination process. Consequently, the ΔV for each maneuver includes the design ΔV ($\Delta V_{BURN} + \Delta V_{TURNS}$) plus any ΔV events related to the maneuver, such as the ΔV from RCS firing to maintain attitude control deadband limits (deadbanding). This sum of design ΔV and associated ΔV events will be herein referred to as the expected ΔV .

A second issue is the choice of coordinate system for expressing the errors. Since each maneuver ΔV is in a different inertial direction yet is controlled by the onboard cut-off algorithm and attitude control subsystem, spacecraft body-fixed coordinates are a natural choice for analyzing the execution errors. A spacecraft coordinate frame already exists for Cassini, as seen in Figure 13: $X_{S/C}$, $Y_{S/C}$, and $Z_{S/C}$. The $Z_{S/C}$ axis points from the high gain antenna to the main engine, the $X_{S/C}$ axis points away from where Huygens was attached, and the $Y_{S/C}$ axis completes the right-handed system. However, a coordinate system with an axis parallel to the expected ΔV is preferred. The compromise is the thrust-vector-control (TVC) coordinate frame with Z_{TVC} parallel to the expected ΔV , X_{TVC} parallel to the projection of $X_{S/C}$ onto the plane perpendicular to Z_{TVC} , and Y_{TVC} completing the right-handed system. The plane perpendicular to

Z_{TVC} is referred to herein as the pointing plane. With this type of coordinate frame, execution errors can be expressed with two perpendicular components, magnitude and pointing. Magnitude errors are computed simply by differencing the lengths of the reconstructed and expected ΔV vectors. Pointing errors are the vector differences of the reconstructed and expected ΔV s projected onto the pointing plane. They are given in X_{TVC} and Y_{TVC} components in m/s as they represent ΔV errors. Use of angular units is reserved for the proportional component of the pointing errors.

The main engine uses an onboard accelerometer to measure ΔV_{BURN} . The accelerometer scales its data with the scale factor, producing an acceleration measurement. Those measurements are accumulated to provide increments of ΔV ; the burn is terminated when the commanded ΔV is achieved. The accelerometer scale, therefore, affects the executed ΔV . If it is too large, the executed ΔV will be too small, and vice-versa. The ratio of the estimated accelerometer scale factor to the onboard value can be used to correct the expected ΔV of main engine burns:

$$\Delta V_{corr. \text{ expected}} = \Delta V_{\text{expected}} + (c_{MEA} - 1)\Delta V_{BURN}, \quad (6)$$

where c_{MEA} is the accelerometer scale factor correction ratio ($c_{MEA} = \frac{\text{Estimated Acc. S. F.}}{\text{Onboard Acc. S. F.}}$). This ratio will be equal to 1 for maneuvers that were executed using the latest estimate of the accelerometer scale factor.

Unlike for main engine, ΔV s for RCS maneuvers are computed via a virtual accelerometer, which measures increments of time, not ΔV . Increments of burn time are converted to increments of ΔV via the classical rocket equation, which is where the onboard thrust primarily influences the algorithm. When the accumulation of these increments reaches the desired ΔV , the burn is cut off. Hence, if the onboard thrust value is too large, than the executed ΔV_{BURN} will be too small, and vice-versa. Discrepancies between the onboard and predicted thrust values have usually been due to either onboard values not being updated since the previous maneuver or onboard values being updated with earlier predicts. Operationally, these differences have been eliminated starting with OTM-100, when ground software started automatically providing spacecraft commands to update the thrust with the latest predicted value. In order to correct the expected ΔV maneuver, the predicted thrust should be accounted for. Analogous to c_{MEA} , this is accomplished by computing the ratio of the predicted thrust value to the onboard thrust value and applying it to the RCS burn ΔV :

$$\Delta V_{corr. \text{ expected}} = \Delta V_{\text{expected}} + (c_{RCS} - 1)\Delta V_{BURN}, \quad (7)$$

where c_{RCS} is the thrust correction ratio ($c_{RCS} = \frac{\text{Predicted Thrust}}{\text{Onboard Thrust}}$). Using this ratio to correct the ΔV assumes linearity of ΔV with thrust.

ACKNOWLEDGMENTS

This research was carried out at the Jet Propulsion Laboratory, California Institute of Technology, under a contract with the National Aeronautics and Space Administration. © 2013 California Institute of Technology. Government sponsorship acknowledged.

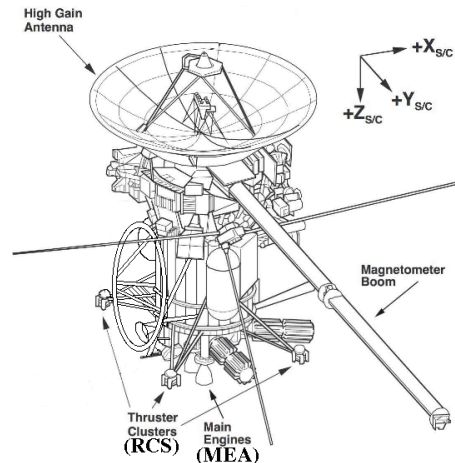


Figure 13: Cassini-Huygens Spacecraft

References

- [1] S. V. Wagner and T. D. Goodson, "Execution-Error Modeling and Analysis of the Cassini-Huygens Spacecraft Through 2007," *AAS/AIAA Space Flight Mechanics Meeting*, AAS Paper 08-113, Galveston, TX, January 27–31, 2008.
- [2] C. R. Gates, "A Simplified Model of Midcourse Maneuver Execution Errors," Tech. Rep. 32-504, NASA Jet Propulsion Laboratory, Pasadena, CA, October 15, 1963.
- [3] S. V. Wagner and J. Arrieta, "2012-1 Cassini Main Engine Maneuver Execution-Error Model," JPL IOM 343C-12-004A, September 5, 2012.
- [4] J. B. Jones, S. M. Ardalan, T. T. Zorn, and K. W. Kloster, "A-Branch Z-Facing Thrust Magnitude Estimation," JPL IOM 3430-10-014, March 24, 2010.
- [5] M. Mizukami, T. J. Barber, L. N. Christodoulou, C. S. Guernsey, and W. A. Haney, "Cassini Spacecraft Reaction Control System Thrusters Flight Experience," *57th JANNAF Propulsion Meeting*, Colorado Springs, CO, May 2010.
- [6] S. V. Wagner, "2012-1 Cassini RCS Maneuver Execution-Error Model," JPL IOM 343C-12-005, September 13, 2012.
- [7] S. V. Wagner, J. Arrieta, Y. Hahn, P. W. Stumpf, P. N. Valerino, and M. C. Wong, "Cassini Solstice Mission Maneuver Experience: Year Three," *AAS/AIAA Astrodynamics Specialist Conference*, AAS Paper 13-717, Hilton Head, SC, August 11–15, 2013.
- [8] T. D. Goodson, "Execution-Error Modeling and Analysis of the GRAIL Spacecraft Pair," *AAS/AIAA Space Flight Mechanics Meeting*, AAS Paper 13-268, Hilton Head, SC, August 11–15, 2013.
- [9] S. V. Wagner, "Maneuver Execution-Error Model 2008-01 Recommendation," JPL IOM 343C-09-001, January 9, 2009.
- [10] S. V. Wagner and D. C. Roth, "Request for Adjustment of FADJ Factor to Remove Observed Cassini RCS (B-Branch) Proportional-Magnitude Bias," JPL IOM 343C-12-007, August 20, 2012.
- [11] S. V. Wagner, J. Arrieta, C. G. Ballard, Y. Hahn, P. W. Stumpf, and P. N. Valerino, "Cassini Solstice Mission Maneuver Experience: Year One," *AAS/AIAA Astrodynamics Specialist Conference*, AAS Paper 11-528, Girdwood, AK, July 31–August 4, 2011.
- [12] T. A. Burk, "Cassini Orbit Trim Maneuvers at Saturn Overview of Attitude Control Flight Operations," *AIAA Guidance, Navigation, and Control Conference*, Portland, OR, August 8–11, 2011.
- [13] D. L. Gray, "Main Engine Proportional Accuracy Estimates," JPL IOM 312.H-00-002, April 20, 2000.
- [14] J. B. Jones and J. L. Webster, "Maneuver Execution-Error Model 2006-01 Recommendation," JPL IOM 3430-06-018, March 30, 2006.
- [15] T. D. Goodson, "Maneuver Execution-Error Model 2007-01," JPL IOM 343C-07-005, August 21, 2007.
- [16] R. V. Hogg and E. A. Tanis, *Probability and Statistical Inference*. New York: Macmillan Publishing Company, fourth ed., 1993.